Modeling of quasi-tapered microstrip antenna based on expansion-exponential tapered method and its application for wideband MIMO structure

by Teguh Firmansyah

Submission date: 26-Jun-2023 01:07PM (UTC+0700)
Submission ID: 2122800637
File name: 1-s2.0-S1434841123002194-main.pdf (8.41M)
Word count: 8839
Character count: 45722

Int. J. Electron. Commun. (AEÜ) 169 (2023) 154745

Contents lists available at ScienceDirect

International Journal of Electronics and Communications

journal homepage: www.elsevier.com/locate/aeue

Regular paper

Modeling of quasi-tapered microstrip antenna based on expansion-exponential tapered method and its application for wideband MIMO structure

Teguh Firmansyah [a,*], Supriyanto Praptodiyono [a], Jaka Permana [a], Syah Alam [b], Toto Supriyanto [c], Ken Paramayudha [d], Yuyu Wahyu [d], Mudrik Alaydrus [e], Jun Kondoh [f,g]

[a] Department of Electrical Engineering, Universitas Sultan Ageng Tirtayasa, Cilegon, Indonesia
[b] Department of Electrical Engineering, Universitas Trisakti, Jakarta, Indonesia
[c] Department of Telecomunication Engineering, Politeknik Negeri Jakarta, Jakarta, Indonesia
[d] Research Center for Electronics and Telecommunication, Indonesian Institute of Sciences, Bandung, Indonesia
[e] Department of Electrical Engineering, Universitas Mercu Buana, Jakarta, Indonesia
[f] Graduate School of Science and Technology, Shizuoka University, 3-5-1 Johoku, Naka-ku, Hamamatsu-shi 432-8561, Japan
[g] Graduate School of Integrated Science and Technology, Shizuoka University, 3-5-1 Johoku, Naka-Ku, Hamamatsu-shi, Shizuoka 432-8561, Japan

ARTICLE INFO

Keywords:
4G/WLAN/X-band/5G
Expansion-exponential
MIMO antenna
Quasi-tapered structure

ABSTRACT

In this paper, a quasi-tapered wideband antenna using a circular-shaped with an inverted-omega ground structure is presented. A tapered antenna is usually developed based on linear-shape, exponential-shape, or Klopfenstein-shape tapper. Here, we proposed an expansion of the exponential tapered model to investigate the circular-shaped tapered structure. In detail, the proposed antenna is divided into circular divergent and circular convergent-tapered sections. Then, the impedance ratio is utilized to analyze the tapered structure. Moreover, the ABCD parameter based on the transmission line model is used to investigate the overall antenna structure. The proposed model was verified by finite element method and a step impedance resonance evaluation. Furthermore, the proposed wideband antenna is also developed with multiple input multiple output (MIMO) and mutual coupling reduction structure. The antenna was fabricated on Rogers RT/Duroid 5880 substrate with $\varepsilon_r = 2.2$, thickness of $h = 1.6$ mm, and dielectric loss tan $d = 0.0009$. As a result, the proposed MIMO antenna can successfully cover the 4G (3.3 GHz), mid-band 5G (3.4–3.8 GHz), WLAN (5.8 GHz), X-band (10–11 GHz), and high-band 5G (24.5–26 GHz) communications. A good agreement between the simulated and measured results validates the proposed method.

1. Introduction

A massive communication network with high data-rate capability is required to support 5G technology [1,2]. This challenging requirement has forced the development of 5G technology to work at the millimeter-wave (mmW) band to accommodate an enormous number of users with a wide bandwidth availability [3,4]. Several interesting methods of wideband antenna design working at mmW band have been investigated such as the substrate integrated cavity (SIC) antenna [5] and double-sided substrate-integrated waveguide (SIW) antenna [6]. They operate at the mmW band with a gain of 12 dBi and 8 dBi, respectively. Moreover, a monopole-like antenna structure [7] and a magneto-electric antenna [8] were introduced to combine 4G/WLAN and 5G communications. Furthermore, antennas based on a tapered structure were proposed in [9–12].

In addition, another fundamental characteristic of 5G antennas is the multiple-input multiple-output (MIMO) capability. A well-designed MIMO antenna should deliver excellent particular performances, such as mutual coupling (MC), envelope correlation coefficient (ECC), and diversity gain (DG) [13–15]. Several methods were proposed for development of MIMO antennas including quasi-Yagi structure [16], metal frame structure [17], vertical stubs [18], fractal [19], and Y-shape structure [20]. Nonetheless, although these methods offer a good MIMO performance, they were only applicable for a single band 5G application. Then, a dual-loop antenna structure [21], step impedance [22], and a double-oval shaped antenna [23] were introduced for 4G and 5G

* Corresponding author.
E-mail address: teguhfirmansyah@untirta.ac.id (T. Firmansyah).

https://doi.org/10.1016/j.aeue.2023.154745
Received 7 March 2023; Accepted 24 May 2023
Available online 2 June 2023

implementation with MIMO capability [24,25]. Nevertheless, these antennas did not target the mmWave band. Therefore, we can see the gap in the development of the MIMO antenna that can handle 4G, WLAN, X-band, and mid-high band 5G communications from S-band to mmW-band.

In addition to wideband performance and MIMO capability, the modeling of an antenna is essential for understanding and investigating its behavior. Therefore, many researchers proposed and derived models for antennas based on recursive convex optimization [26], equivalent circuit modeling [27], cavity model [28], and stepped-impedance resonator [29]. However, these proposed modeling techniques were focused on a narrow bandwidth antenna. To model wideband antennas, other methods such as space-mapping with kriging surrogates [30], linear elements [31], equivalent circuit model [32] have been successfully applied with slightly complex calculations. Furthermore, the MIMO antenna applications were investigated using various modeling techniques, namely a statistical analysis model [33], equivalent circuit model [34], effective length matrices [35], and eigen-analysis [36]. Nevertheless, these models were applied for narrowband applications. It is important to note that the design of antennas with wideband characteristics and suitable MIMO capability remains an open issue in antenna engineering. The study presented in this paper made several contributions, which are listed as follows:

1. A wideband antenna based on a quasi-tapered structure using a circular shape is proposed. A quasi-tapered characteristic was obtained by integrating a circular-shaped patch antenna with an inverted omega ground plane as shown in Fig. 1(a).
2. We also proposed an expansion-exponential tapered model to investigate the quasi-tapered structure based on a circular shape. This proposed model was utilized due to the limitation of the traditional linear, exponential, and Klopfenstein tapering methods. It is important to note that our circular tapered structure diverges from the conventional linear, exponential, or Klopfenstein shapes typically employed in tapering.
3. To obtain the mathematical model of for the circular shape tapered structure, we expand the the existing exponential shape tapered model. In detail, Fig. 1(b) illustrates the proposed circular tapered structure which is divided into two halves circular shapes. It is seen that the physical dimension of the left-side of the half-circular shape is increasing. However, if we investigate the impedance characteristic, the impedance value is decreasing. Therefore, the left side structure has a convergent behavior. Vice versa, the right side of the half-circular shape has a divergent characteristic.
4. The study employs the ABCD parameter based on the transmission line model to investigate the overall antenna structure. The proposed model was verified by the finite element method (FEM). Following the verification process, the proposed antenna was then applied in a MIMO structure. The fabrication of the antenna was carried out on a Rogers RT/Duroid 5880 substrate with $\varepsilon r = 2.2$, thickness of $h = 1.6$ mm, and dielectric loss tan $\delta = 0.0009$.
5. In addition, we also proposed a multislot defected ground structure (DGS) structure to reduce the mutual coupling parameter in the MIMO antenna system. As a result, the proposed MIMO antenna demonstrated wide bandwidth and excellent performance across various communication bands. The antenna is capable of operating in the S-band to mmW band, effectively covering a broad frequency range. This wide frequency coverage enabled the antenna to support multiple communication standards, including 4G (3.3 GHz), mid-band 5G (3.4–3.8 GHz), WLAN (5.8 GHz), and high-band 5G (24.5–26 GHz) concurrently. Table 1 provides an overview of the proposed research positioning.

This article has structures as follows. The first section describes the research position and the proposed method. The second section focuses on the quasi-tapered investigation based on the convergent/divergent-tapered model with ABCD parameters. The third section highlights the design and measurement of the proposed quasi-tapered MIMO antenna. Then, it is followed by the results/discussions and the MIMO performance investigation. Finally, the last section concludes this research.

2. Quasi-tapered antenna based on circular-shaped patch with inverted-omega ground structure

Several methods have been studied to predict the operation frequency of an antenna, namely the lumped circuit modelling [40,41] and the transmission line approach [13]–[17]. Fig. 1(a) shows the main part of the antenna structure including the patch plane, ground plane, and excitation port. It should be noted that the proposed antenna has a direct excitation configuration. Hence, we can extract the antenna structure as several parts: a source impedance (Z_S), an excitation line, a convergent-tapered section, a divergent-tapered section, and a load-impedance (Z_L). Here, we use air impedance as the load impedance [42,43], as depicted in Fig. 1(b). The followed section describes the expanded exponential-shape tapper to get the circular-shape tapper model.

2.1. Half-circular shaped tapered with expansion-exponential tapered model

The proposed half-circular shape tapered configuration with the expansion-exponential tapered model is shown in Fig. 2(a). It has a radius of R and has a convergent-tapered behavior. The input part will directly connected to the source impedance of $Z_{S(2)}$ and the end part is connected to the load impedance of $Z_{L(2)}$. It has a length of l_A from the

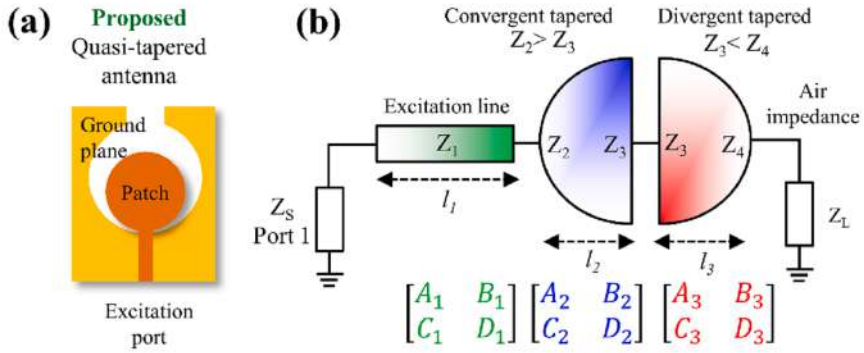

Fig. 1. (a) the proposed antenna based on quasi-tapered structure using circular-shaped patch with inverted-omega ground, (b) the ABCD parameters of proposed quasi-tapered antenna based on exponential tapered transmission lines approach.

Table 1
Research position.

Ref	Freq. (GHz)	Antenna structure	Proposed methods	Applications		MIMO antenna	Mutual coupling reduction	Advantages
				Narrow-band	Wide-band			
[26]	2.50	Microstrip slot dipole	Recursive convex optimization	Yes	–	–	–	The proposed model has the capability to make predictions for the near field.
[27]	30.0	Micro-coaxial collinear	Equivalent circuit modeling	Yes	–	–	–	The calculation model is capable of identifying the equivalent circuit.
[28]	2.47–2.56	Stacked Microstrip Ring	Cavity model	Yes	–	–	–	The proposed model can predict the near field.
[29]	1.50–2.50	Stepped-Impedance Slot Antenna	Stepped-Impedance Resonator	Yes	–	–	–	The proposed model is capable of predicting the dualband impedance characteristics.
[30]	2.00–8.00	CPW-fed slot antenna with monopole	Space-mapping with kriging surrogates	–	Yes	–	–	The proposed model has the ability to forecast the value of reflection coefficient.
[31]	3.00	Conventional dipole	Linear elements	–	Yes	–	–	The model can estimate the radiation pattern.
[32]	2.51–6.55	Linear tapered slot	Equivalent circuit model	–	Yes	–	–	The calculation model has the potential to determine the equivalent circuit.
[33]	3.50–8.50	Monopole UWB	Statistical analysis model	–	Yes	–	–	The proposed model can make predictions for the value of reflection coefficient.
[34]	2.20	Monopole	Equivalent circuit model	Yes	–	Yes	–	The network parameters can be utilized for the prediction of S-parameters performance.
[35]	5.15–5.35	Monopole	The effective length matrices	Yes	–	Yes	–	The effective length matrices demonstrate good agreement with the method of moments.
[36]	5.20	FIFA-monopole	Eigen-Analysis	Yes	–	Yes	–	The model can determine the radiation pattern.
[37]	2.90–18.00	Circular shaped monopole	N.R.	–	Yes	Yes	Yes	The proposed antenna exhibits wideband performance.
[38]	3.00 – 30.0	Monopole with slot	N.R.	–	Yes	Yes	Yes	The proposed antenna possesses good isolation.
[39]	3.30 –8.50	L-shaped branch	N.R.	–	Yes	Yes	Yes	The proposed antenna has wideband performance.
This paper	3.30–26.0	Quasi-tapered using circular shaped	Expansion-exponential tapered model	–	Yes	Yes	Yes	The proposed antenna design combines wideband performance, a simple impedance calculation model, and low mutual coupling in a MIMO configuration.

Note: N.R = not reported.

input-port to the output-port. Moreover, Fig. 2(b). show the approximation characteristic of the impedance ratio (K) with different length of the taper. Here, we used the widest dimension of taper as the reference hence it has a unity value. Then, we can see that the impedance is increasing due to the decrease in the taper width.

To investigate the half-circular tapered configuration, we expand the exponential tapered model by introduce the term of impedance ratio with the expansion-exponential tapered model. The K can be written as:

$$K = a\left(e^{b(1-l_A)} + c\right) \tag{1}$$

where the a, b, and c are the adjustable constant parameters that follow the impedance curve of the circular shape. The intrinsic characteristic of the exponential-taper model is defined by the taper factor (b). Therefore, the impedance value of $Z_{(l=l_A)}$ at the length of l_A can be determined as:

$$Z_{(l=l_A)} = Z_{(l=0)}a\left(e^{b(1-l_A)} + c\right) \tag{2}$$

where $Z_{(l=0)}$ is the impedance at the initial position. Here, we state the initial impedance value as Z_0. Then, the ABCD matrix of the half circular taper can be determined by:

$$\begin{bmatrix} A & B \\ C & D \end{bmatrix} = \frac{1}{\sqrt{Z_A Z_B}} \times \begin{bmatrix} Z_A \cosh\gamma l_A - Z_A \frac{d}{2\gamma}\sinh\gamma l_A & jZ_A Z_B \frac{\beta}{\gamma}\sinh\gamma l_A \\ j\frac{\beta}{\gamma}\sinh\gamma l_A & Z_B \cosh\gamma l_A + Z_B \frac{d}{2\gamma}\sinh\gamma l_A \end{bmatrix} \tag{3}$$

where

$$\gamma = \sqrt{\beta^2 - \left(\frac{d}{2}\right)^2} \tag{4}$$

$$d = \frac{\ln\left(a\left(e^{b(1-l_A)} + c\right)\right)}{l_A} \tag{5}$$

$$\beta = \frac{2\pi}{\lambda} \tag{6}$$

with γ is the propagation constant. Moreover, the input impedance $Z_{IN(A)}$ can be calculated as:

$$Z_{IN(A)} = Z_A \frac{2Z_L\gamma + (j2Z_B\beta - Z_L d)\tanh\gamma l_A}{2Z_B\gamma + (j2Z_L\beta + Z_B d)\tanh\gamma l_A} \tag{7}$$

The next step is to investigate the antenna structure using the expansion-exponential taper model approximation, as depicted in Fig. 3 (a)-(b).

2.2. Quasi-tapered antenna with expansion-exponential tapered model

In detail, the proposed antenna structure can be separated into three important parts including excitation line, convergent-taper, and divergent taper, as shown in Fig. 3(a). It is important to note that eventhough the physical dimension becomes narrow or converging the impedance value becomes higher or diverging. Therefore, we called it as a divergent-taper and vice versa. Fig. 3(b) shows that the excitation line width is constant. Therefore, the impedance ratio is also constant. In addition, we introduce K_1 and K_2 as the impedance ratio for convergent-taper and divergent-taper, respectively. In detail, the investigation of the structure will be started by the excitation line followed by the convergent taper and divergent taper.

2.2.1. The excitation line

For more convenience and detail of the tapered structure, we can see Fig. 3(a)-(3b). The excitation line has directly connected to the input

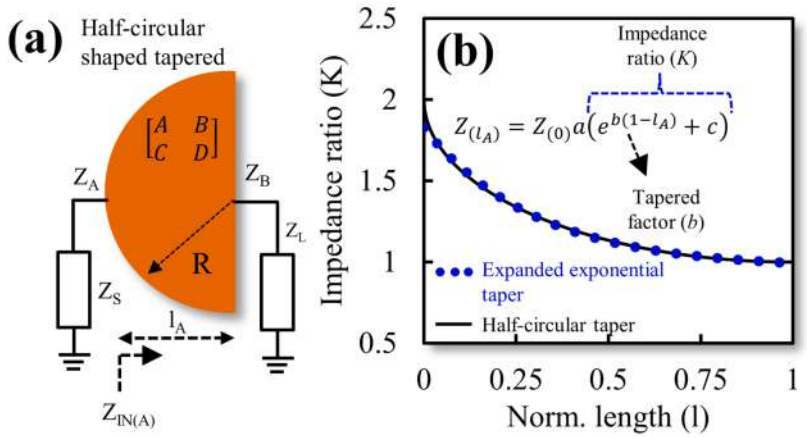

Fig. 2. **(a)** The proposed of half-circular shaped taper configuration with convergent tapered behavior. (b) Approximation of impedance ratio with widest dimension of taper as the reference.

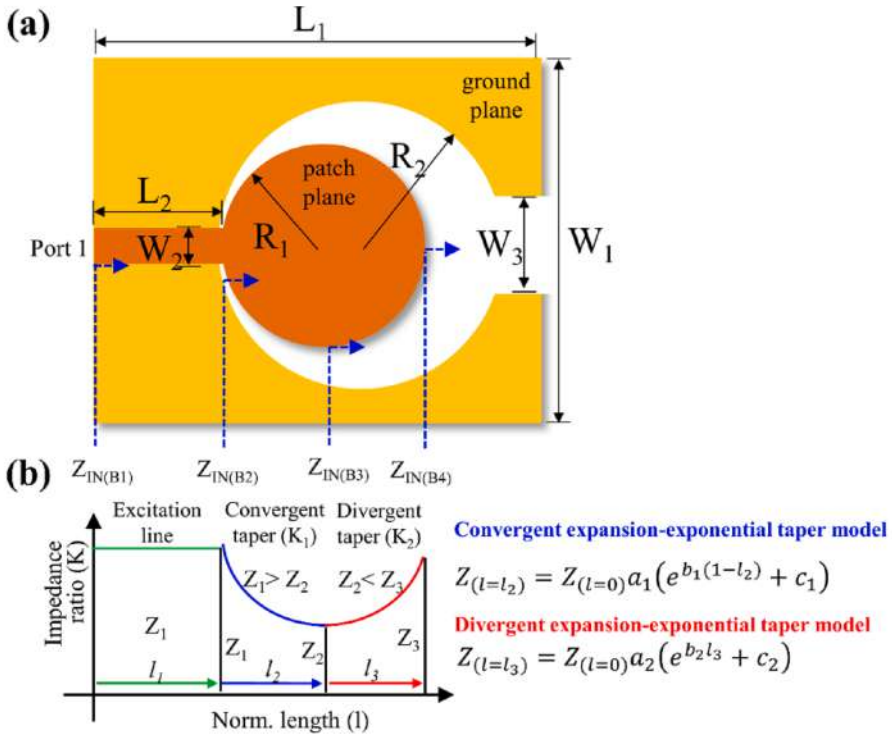

Fig. 3. (a) Quasi-tapered antenna based on circular-shaped with inverted-omega ground structure, (b) the approximation of impedance ratio and the electrical length of the proposed antenna structure.

impedance (Z_S) which is usually called as port 1. Moreover, the excitation line has the impedance characteristic (Z_1) and electrical length (l_1). They correspond to the width (W_2) and the length (L_1), respectively. To simplify the investigation, we assume the impedance of the excitation line (Z_1) is equal to the source impedance (Z_S).

2.2.2. The half-circular shaped convergent-tapered

The convergent-tapered is focused on decreasing of impedance values. Therefore, the impedance ratio (K_1) for the convergent taper of the proposed antenna is determined by:

$$K_1 = a_1\left(e^{b_1(1-l_2)} + c_1\right) \tag{8}$$

where the a_1, b_2, and c_2 are constant parameters and the value follows the impedance curve. Moreover, b_2 is the convergent taper ratio for the proposed antenna.

Then, the impedance value of $Z_{(l=l_2)}$ at the length of l_2 can be calculated as:

$$Z_{(l=l_2)} = Z_{(l=0)} a_1 \left(e^{b_1(1-l_2)} + c_1\right) \tag{9}$$

where $Z_{(l=0)}$ is the impedance at the initial position. The ABCD matrix of half-circular taper with convergent structure can be determined by:

$$\begin{bmatrix} A_2 & B_2 \\ C_2 & D_2 \end{bmatrix} = \frac{1}{\sqrt{Z_1 Z_2}} \times \begin{bmatrix} Z_1 \cosh\gamma_2 l_2 - Z_1 \frac{d_1}{2\gamma} \sinh\gamma_2 l_2 & jZ_1 Z_2 \frac{\beta}{\gamma} \sinh\gamma_2 l_2 \\ j\frac{\beta}{\gamma} \sinh\gamma_2 l_2 & Z_2 \cosh\gamma_2 l_2 + Z_2 \frac{d_1}{2\gamma} \sinh\gamma_2 l_2 \end{bmatrix} \tag{10}$$

where

$$\gamma_2 = \sqrt{\beta^2 - \left(\frac{d_1}{2}\right)^2} \tag{11}$$

$$d_1 = \frac{\ln\left(a_1\left(e^{b_1(1-l_2)} + c_1\right)\right)}{l_2} \tag{12}$$

with γ_2 is the propagation constant of the convergent taper with circular shape. Then, Fig. 4(a)-4(c) show the relation between normalized length (l_2) with the impedance ratio (K_1) for convergent taper with different value of a_1, c_1, and b_1.

In detail, the normalized length of l_2 value was analyzed between 0 and 1. It can be seen that the a_1 and c_1 have a similar effect to the impedance ratio (K_1). The a_1 and c_1 have linear effects to the impedance ratio value. Moreover, K_1 was highly influenced by coefficient b_1. Therefore, by adjusting the value of a_1, c_1, and b_1, we can obtain the impedance ratio that is similar to the circular part.

2.2.3. The half-circular shaped divergent-tapered

The impedance ratio (K_2) for the divergent taper part of the proposed antenna design is determined by:

$$K_2 = a_2\left(e^{b_2 l_3} + c_2\right) \tag{13}$$

where a_1, b_2, and c_2 are the adjustable constant parameters that allows the impedance curve. Moreover, b_2 is the convergent taper ratio for the proposed antenna. The impedance value of $Z_{(l=l_2)}$ at the length of l_2 can be calculated as:

$$Z_{(l=l_3)} = Z_{(l=0)} a_2\left(e^{b_2 l_3} + c_2\right) \tag{14}$$

Then, the ABCD matrix of half-circular taper with convergent structure can be determined by:

$$\begin{bmatrix} A_3 & B_3 \\ C_3 & D_3 \end{bmatrix} = \frac{1}{\sqrt{Z_2 Z_3}} \times \begin{bmatrix} Z_2 \cosh\gamma_3 l_3 + Z_2 \frac{d_2}{2\gamma_3} \sinh\gamma_3 l_3 & jZ_2 Z_3 \frac{\beta}{\gamma_3} \sinh\gamma_3 l_3 \\ j\frac{\beta}{\gamma_3} \sinh\gamma_3 l_3 & Z_3 \cosh\gamma_3 l_3 - Z_3 \frac{d_2}{2\gamma_3} \sinh\gamma_3 l_3 \end{bmatrix} \tag{15}$$

where

$$\gamma_3 = \sqrt{\beta^2 - \left(\frac{d_2}{2}\right)^2} \tag{16}$$

$$d_2 = \frac{\ln\left(a_2\left(e^{b_2 l_3} + c_2\right)\right)}{l_3} \tag{17}$$

with γ_2 is the propagation constant of the circular shape. Moreover, Fig. 5(a)-5(c) show the relation between normalized length (l_2) with the impedance ratio (K_1) of the convergent taper for different value of a_1, c_1, and b_1, respectively. In details, the normalized length l_2 value was plotted from 0 to 1. Then, a_1 is varied from 0.028 to 0.038 with a step value of 0.002. Therefore, we can see that the value of K_1 decreases exponentially.

Overall, by adjusting the values of a_1, b_1, and c_1, we can get the impedance ratio values of half-circular shaped using exponential taper model approach.

3. Comparison model

To verify the proposed model, the comparison of the impedance ratio of the expanded exponential model and finite element method (FEM) is presented in Fig. 6(a). We can see that the models are in good agreement and fit with each other. This means that the proposed model can be used to calculate the impedance ratio of circular-shaped taper. Moreover, the proposed model can be also implemented and verified using simple case, such as when K = 1 and the length of l between 0.5 and 1, d_1 and d_2 will become 0 as shown in Fig. 6(b). The model can be also utilized for the calculation of input impedance of step impedance resonator. In detail, by using $d = 0$ and the loss-less case of $\gamma = j\beta$, it will lead to the equation of input impedance of step impedance resonator as follows:

$$Z_{IN(B1)} = Z_1 \frac{Z_{IN(B2)} + jZ_1 \tan\beta l_1}{Z_1 + jZ_{IN(B2)} \tan\beta l_1} \tag{18}$$

$$Z_{IN(B2)} = Z_1 \frac{Z_{IN(B3)} + jZ_2 \tan\beta l_2}{Z_2 + jZ_{IN(B3)} \tan\beta l_2} \tag{19}$$

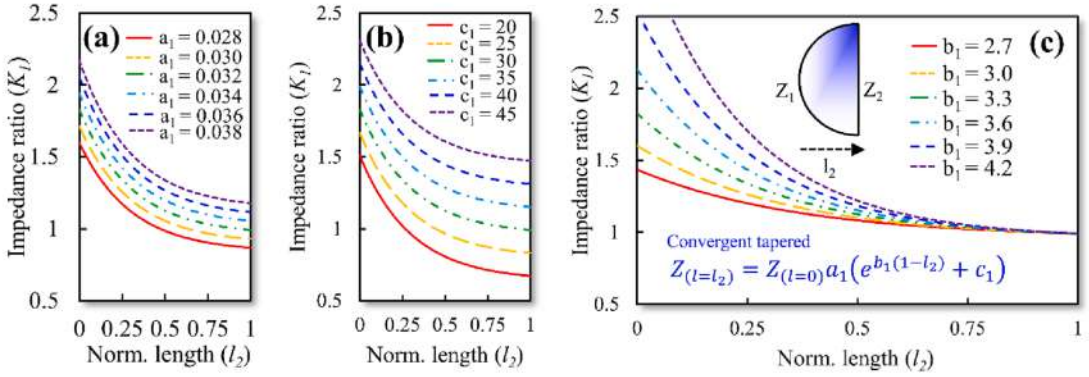

Fig. 4. (a) The relation between normalized length (l_2) with the impedance ratio (K_1) for different value of (a) a_1, (b) c_1, and (c) b_1.

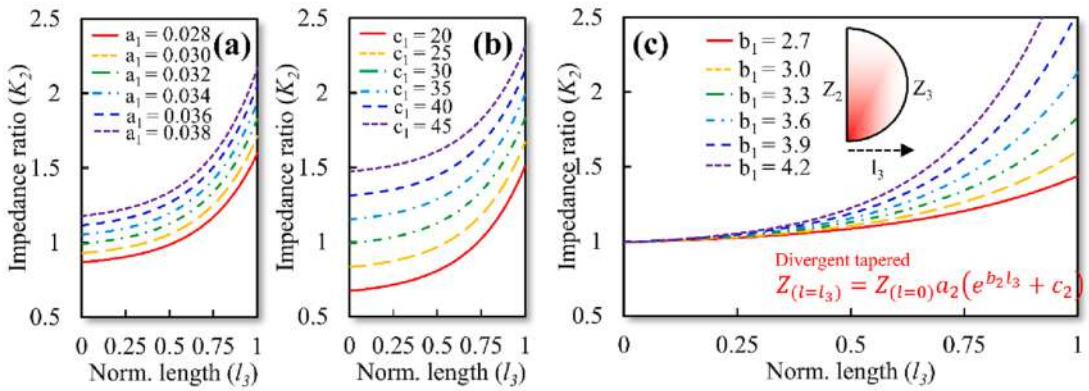

Fig. 5. (a) The relation between normalized length (l_3) with the impedance ratio (K_2) for different value of (a) a_2, (b) c_2 and (c) b_1.

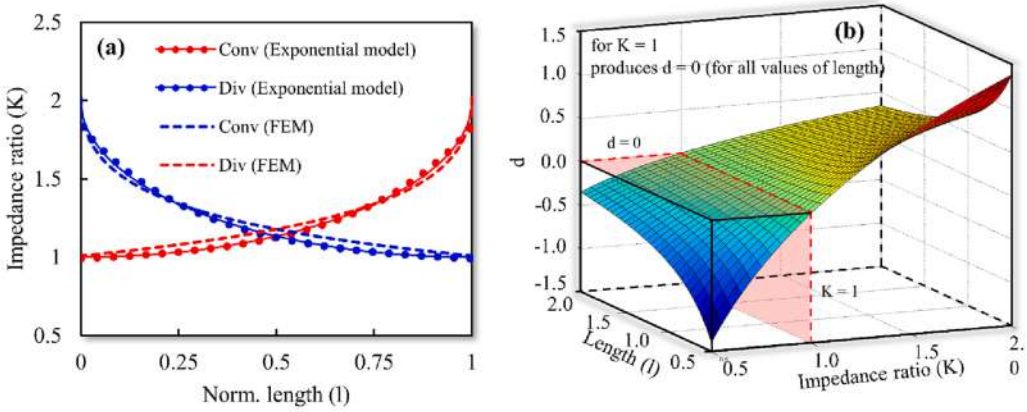

Fig. 6. (a) Comparison of circular shape-tapper using expanded exponential model, and finite element method (FEM) (b) a generalized for case $K = 1$ and its relations between l and d value.

$$Z_{IN(B3)} = Z_2 \frac{Z_{IN(B4)} + jZ_3 \tan\beta l_3}{Z_3 + jZ_{IN(B4)} \tan\beta l_3} \tag{20}$$

$$Z_{IN(B4)} = Z_L \tag{21}$$

Finally, the proposed exponential tapered transmission line model can be used for impedance calculation of circular shape resonator and step impedance resonator.

Fig. 7(a) and 7(b) show the results comparison between the expansion-exponential tapered method and conventional tapered method for circular convergent-taper and circular divergent-taper configurations, respectively. MATLAB software was used to perform the calculations for both the expansion-exponential and conventional tapered methods. In addition to MATLAB, the transmission line electromagnetics modeling tool suite of TNT 1.2.2 was utilized for the FEM based calculations. It is observed that the proposed method exhibited greater consistency and better fit with the FEM results. These results look similar for circular-convergent taper and circular-divergent taper. However, if we compare it with the conventional tapered methods, the deviation is significant. This results suggests that the proposed expansion-exponential tapered method offers distinct advantages and a more suitable design approach compared to conventional methods. Additionally, it is important to note that further detailed investigations of the antenna characteristics were conducted using CST Microwave Studio software.

The next step is antenna dimension optimization and MIMO characterization. The antenna dimension can be optimized to obtain working frequencies ranging from S-band to mmWave band with $|S_{11}| < -10$ dB. To reduce the mutual coupling effect of this proposed MIMO antenna, we include a structure that is based on multi-slot configuration. This multi-slot structure was positioned at the middle part of the antenna ground plane. To evaluate the MIMO performance of the antenna, several additional parameters should also considered. The parameters $|S_{21}|$, ECC, and DG. ECC can be determined using S-parameters [44]. Then, the DG can be derived from the ECC equation [44].

4. Design of quasi-tapered wideband MIMO antenna

The design steps of the proposed antenna can be divided into two main parts. The first part focuses on the modelling of the quasi-tapered antenna using the transmission line model approach. Then, the second part focuses on the optimization of the MIMO antenna. In detail, the design procedures of the quasi-tapered antennas have several steps including a conventional circular shape monopole microstrip antenna design, feeding length modification, and ground-plane modification into an inverted omega-ground structure as illustrated as antenna A#, B#, and C# in Fig. 8(a)-8(c), respectively.

The substrate geometry of antenna A# is rectangular with a length of L_1 and a width of W_1. The radiating part of the antenna A# structure is developed from a circular-shaped patch with radius of R_1 and is fed by a direct-excitation feed with a length of L_{3A} and width of W_2. At the

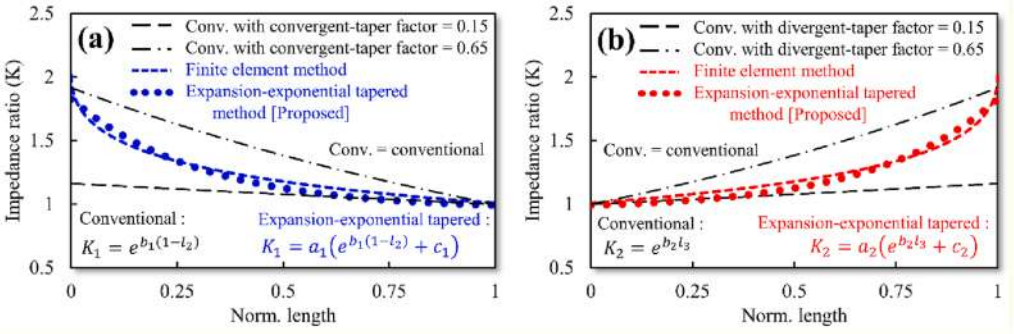

Fig. 7. Results comparison between the proposed method expansion-exponential tapered method and conventional tapered method (a) circular convergent-taper, and (b) circular divergent-taper.

ground plane side, a circular ground slot with the radius of R_2 is included. This ground slot is positioned at distances of L_2 and L_4 from the bottom and the top side of the substrate, respectively. It should be mentioned that the position of the circular patch and the circular ground slot are centrally aligned. Fig. 9(a) shows the reflection coefficient of antenna A# with variation of R_1. In this scenario, R_1 is varied from 3 mm to 15 mm. We can see that the change of R_1 leads to the variation of antenna frequency and the return loss. However, we note that the antenna still has a poor matching impedance at several desired frequencies as shown in the reflection coefficient value. Hence, in the next step we investigate the effect of excitation length (L_2) variation on the resonant frequency as antenna B#. The simulation result of the effect of L_2 variation is shown in Fig. 9(b). The result indicates that the length of L_2 has a significant effect on the return loss of the antenna. Next, we add an upper part slot with a width of W_3. This antenna is called antenna C#.

Fig. 10(a) shows that by using this additional slot, the antenna has a better reflection coefficient compared to antenna B#. Furthermore, Fig. 10(b) shows the comparison of the return loss of antenna A#/B#/C#. We can see that antenna C# has a better reflection coefficient compared to antenna A# or B#. Therefore, we decide to expand antenna C# into a MIMO structure. The design evolution of the MIMO antenna structure is shown in Fig. 11(a), 11(b), 11(c), and 11(d) as MIMO antenna C1#, C2#, C3#, and C4#. The C1# antenna represents a conventional MIMO antenna which comprises two identical antennas without any structural modification as depicted in Fig. 11(a).

In MIMO antenna C2#, an additional single DGS slot-ground structure with a length of L_{D1} and width of W_{D1} is introduced at the top part of the ground plane as depicted in Fig. 11(b). the MIMO antenna C3# has a dual slots ground structure. The additional slot is positioned at the middle part of the ground plane with a length of L_{D2} and a width of W_{D2}, as shown in Fig. 11(c). Finally, a third ground slot is included in MIMO antenna C4#. This slot is introduced at the bottom part of the ground plane with a length of L_{D3} and width of W_{D3}, as illustrated in Fig. 11(d). The complete dimension and 3D view of MIMO antenna C4# can be seen in Fig. 12(a) and Fig. 12(b), respectively.

Moreover, Fig. 13(a) shows the comparison of the reflection coefficient of the MIMO antennas. We can see that a return loss of under −10 dB at the desired frequencies is achieved for all MIMO antennas C1#/C2#/C3#/C4#. This indicates that the proposed MIMO configurations have no significant effect on the operation frequency of the antenna. Lastly, Fig. 13(b) shows the comparison of the mutual coupling of MIMO antenna C1#/C2#/C3#/C4#. The results indicate that the MIMO antenna C4# provides the best isolation with a mutual coupling lower than −20 dB. Next, the proposed antenna is fabricated and measured to verify the simulation results.

5. Result and discussion

The proposed antennas C# and C4# were fabricated on Rogers RT/Duroid 5880 substrate with $\varepsilon_r = 2.2$, thickness of $h = 1.6$ mm, and dielectric loss tan $d = 0.0009$. The complete dimensions are as follows (in millimeter): $R_1 = 9$, $R_2 = 15$, $W_1 = 40$, $W_2 = 2.6$, $W_3 = 10$, $W_T = 85$,

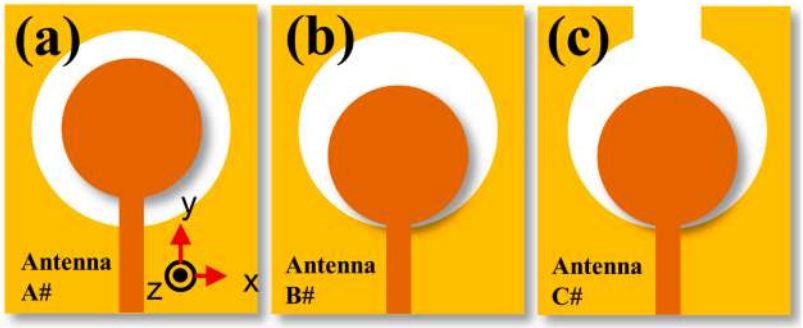

Fig. 8. (a) Conventional circular shape antenna, (b) modification the feeding length of L_2, (c) modification of ground-plane and became inverted omega-ground structure by added W_3.

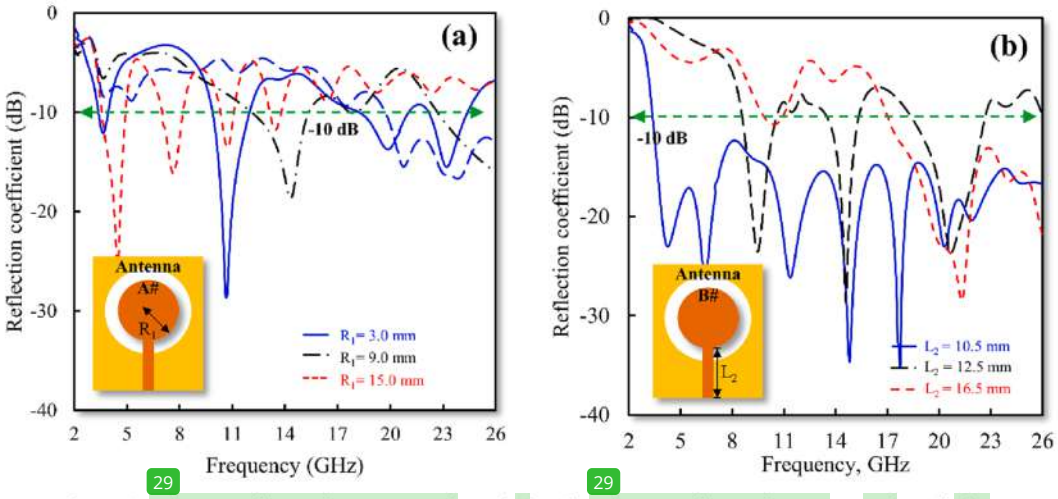

Fig. 9. (a) Reflection coefficient of antenna A# with varied of R_1, (b) Reflection coefficient of antenna B# with varied of L_2.

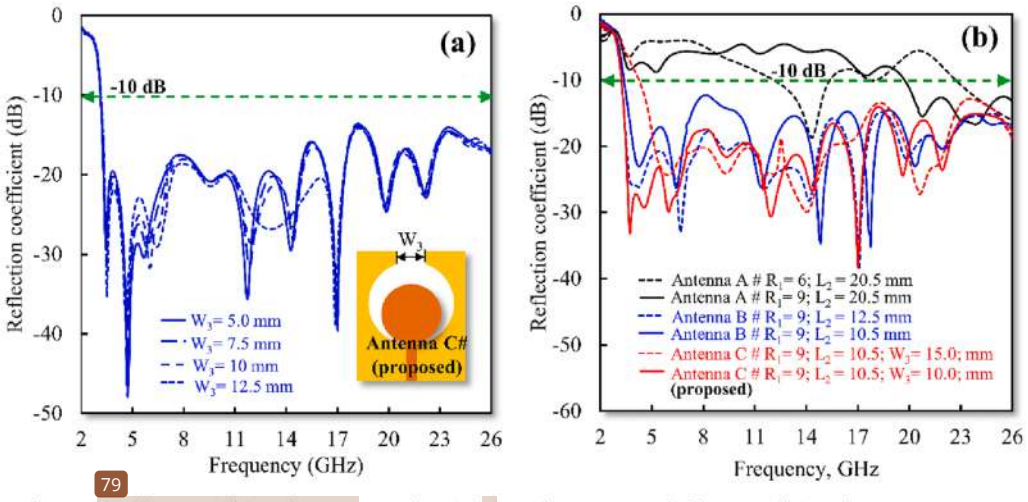

Fig. 10. (a) Reflection coefficient of antenna C# with varied of W3, (b) comparison of reflection coefficient of antenna A#/B#/C#.

$W_{D1} = 5$, $W_{D2} = 5$, $W_{D3} = 5$, $L_1 = 45$, $L_2 = 10.4$, $L_3 = 4.6$, $L_{3A} = 15.5$, $L_{3B} = 10.5$, $L_{D1} = 6$, $L_{D2} = 29.5$, $L_{D3} = 5$. In detail, Fig. 14(a), 14(b), 14(c), and 14(d) show the photographs of fabricated antenna C# and C4# with view from the patch and the ground side. The measurement of the proposed antenna's performance up to 26 GHz was facilitated by using the first-generation of super SMA female connectors from HASCO. Based on the data sheet, this connector has good performance from DC up to 27 GHz [45]. Furthermore, an R&S ZVA67 VNA is used to measure the antenna performance.

Fig. 14(e) shows the reflection coefficient comparison between the simulation and measurement of antenna C#. We can see that at several frequencies points the measured return losses are higher than those from the simulation. Nevertheless, they are still under −10 dB and hence the antenna C# can successfully cover a wide range from S-band to mmW band. Fig. 14(f) shows a comparison of the reflection coefficient between the simulation and measurement of MIMO antenna C4#. In line with the antenna C#, the MIMO configuration does not change the reflection coefficients significantly. The return loss of the proposed MIMO antenna is still under −10 dB.

The mutual coupling (MC) comparison between simulation and measurement of MIMO antenna C4# is depicted in Fig. 14(g). In MIMO antenna, MC is generally used to evaluate the interaction of the antennas. We can see that the MIMO antenna C4# has MC values lower than −20 dB in all desired frequencies. Therefore, we can conclude that the interferences between antennas are insignificant. It should be noted that, in principle, this antenna has the potential to operate across wide frequency bands. However, in this paper, the focus was directed towards specific frequency bands in order to position the study within the context of future communication technologies. We have selected several specific bands such as the 4G (3.3 GHz), mid-band 5G (3.4–3.8 GHz), WLAN (5.8 GHz), X-band (10–11 GHz), and high-band 5G (24.5–26 GHz) communications.

Fig. 15 (a-j) presents the normalized co-and cross-polarization radiation patterns of the proposed antenna. Specifically, Fig. 15 (a-e) display

Fig. 11. (a) MIMO antenna C4#, and (b) 3D view of proposed MIMO antenna C4#.

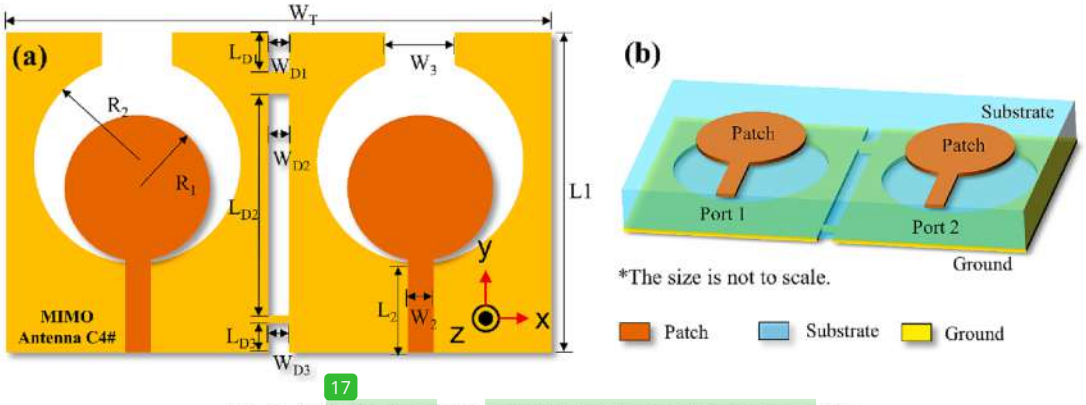

Fig. 12. (a) MIMO antenna C4#, and (b) 3D view of proposed MIMO antenna C4#.

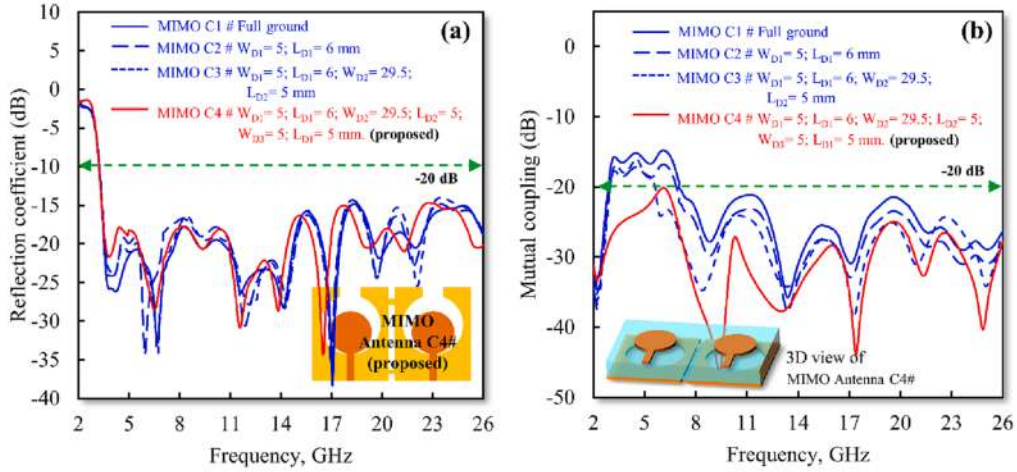

Fig. 13. (a) A comparison of reflection coefficient of MIMO antenna C1#/C2#/C3#/C4#, (b) comparison of mutual coupling of MIMO antenna C1#/C2#/C3#/C4#.

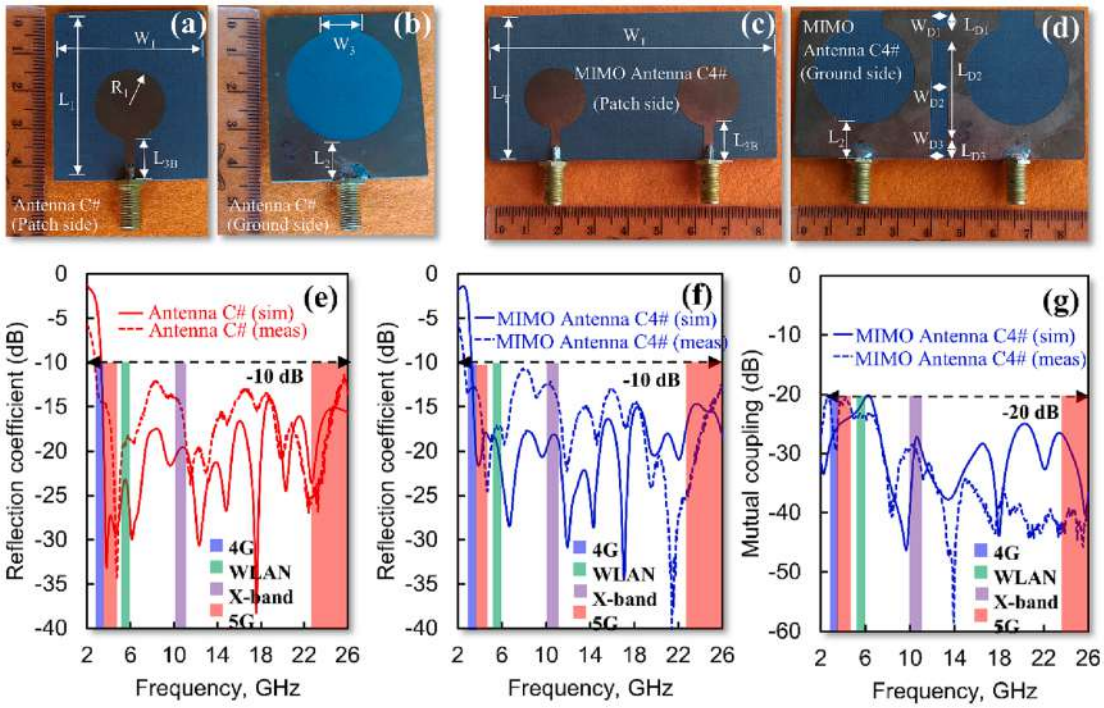

Fig. 14. (a) Fabrication result of antenna C# (a) view from patch side, (b) view from ground side. Fabrication result of MIMO antenna C4# (c) view from patch side, (d) view from ground side. The reflection coefficient comparison between simulation and measurement of (e) antenna C#, (f) MIMO antenna C4#, (g) a mutual coupling comparison between simulation and measurement of MIMO antenna C4#.

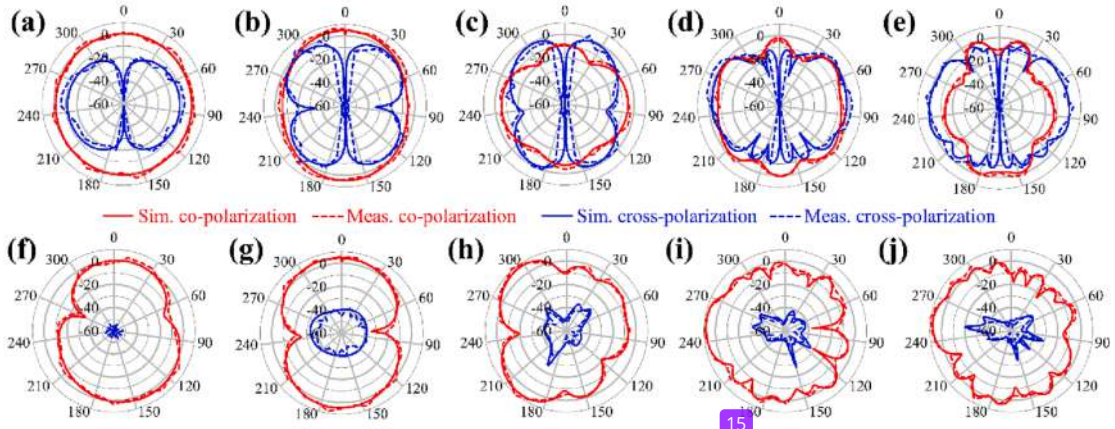

Fig. 15. Co– and cross-polarization normalized radiation patterns at XOZ-plane at frequency of (a) 3.3 GHz, (b) 5.8 GHz, (c) 10 GHz, (d) 24 GHz, and (e) 26 GHz. Then, Co– and cross-polarization normalized radiation patterns at YOZ-plane at frequency of (f) 3.3 GHz, (g) 5.8 GHz, (h) 10 GHz, (i) 24 GHz, and (j) 26 GHz.

the normalized co– and cross-polarization radiation patterns at the XOZ-plane for frequencies of 3.3 GHz, 5.8 GHz, 10 GHz, 24 GHz, and 26 GHz, respectively. It is seen at the XOZ-plane, the cross-polarization values are relatively large. However, the main beam at 0 degree exhibits a very low cross-polarization value. Moreover, Fig. 15 (a-e) show the normalized co– and cross-polarization radiation patterns at YOZ-plane for frequencies of 3.3 GHz, 5.8 GHz, 10 GHz, 24 GHz, and 26 GHz, respectively. At the YOZ-plane direction, the proposed antenna exhibits a very low cross-polarization value. Therefore, it can be concluded the proposed antenna has omni-directional pattern at the YOZ-plane.

As an additional explanation, there are several reasons that the monopole antenna can generate circular polarization such as ground-plane's position and antenna shape [46–48]. The ground-plane plays an important role in determining the polarization of an antenna. In the specific case of a monopole antenna, the ground plane can cause the polarization of the signal to change from its original orientation, with a larger ground plane providing more reflection and resulting in a more significant change in polarization [46–48].

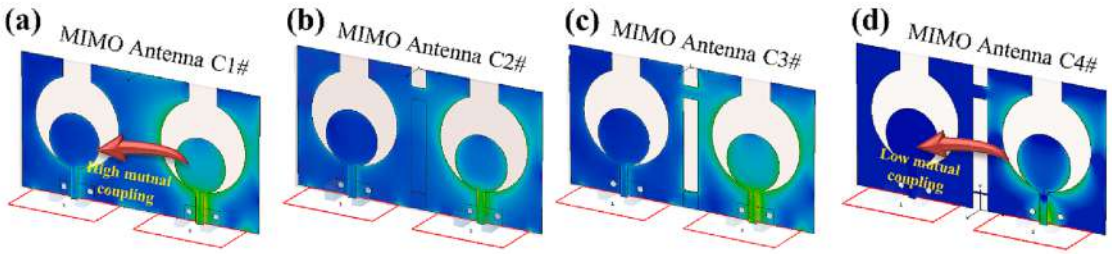

Fig. 16. Surface current density of (a) MIMO antenna C1#, (b) MIMO antenna C2#, (c) MIMO antenna C3#, (d) MIMO antenna C4#.

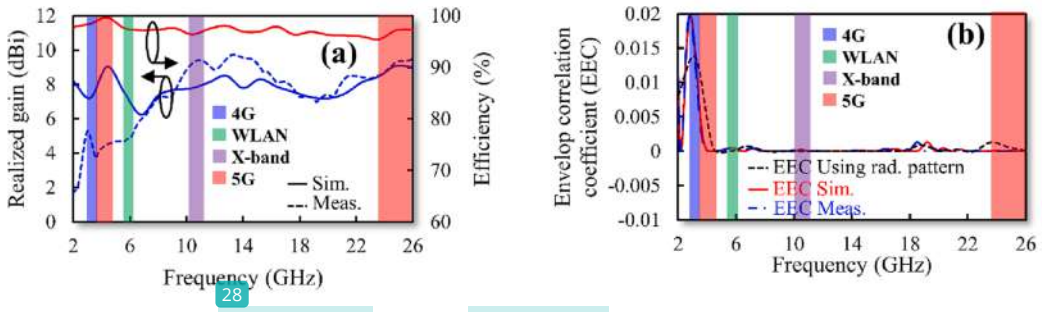

Fig. 17. Comparison result of (a) realized gain and efficiency, (b) enveloped correlation coefficient.

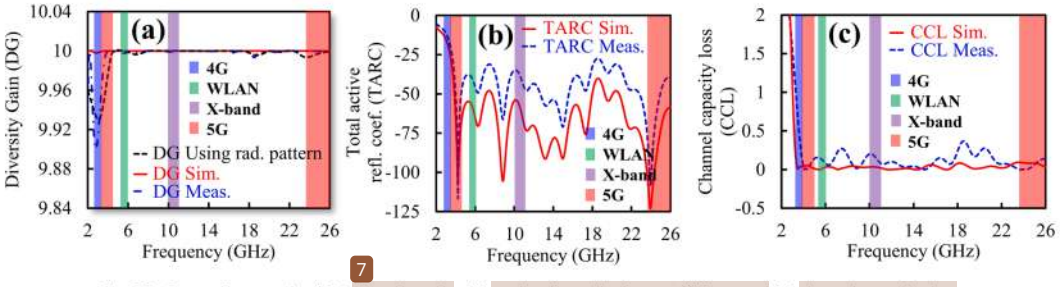

Fig. 18. Comparison result of (a) diversity gain, (b) total active reflection coefficient, and (c) channel capacity loss.

6. MIMO performances

The evaluation of surface current density distribution is crucial to understand the behavior of the proposed MIMO antenna. This surface current density distribution be used to explain the MC between closely spaced antennas. Fig. 16(a), 16(b), 16(c), and 16(d) illustrate the surface current density of MIMO antenna C1#, C2#, C3#, and C4#, respectively. We can see that the MIMO antenna C1# has the highest mutual coupling among others. The MCs are qualitatively decreased after ground slots were included. This can be seen in Fig. 16(d) where the MIMO antenna C4# generates the lowest mutual coupling, as indicated by the blue color in the subsequent antenna. Then, Fig. 17 (a-b) show the results comparison of realized gain and efficiency, and enveloped correlation coefficient, respectively.

A realized gain and efficiency of MIMO antenna C4# shown in Fig. 17(a). As depicted in the graph, the antenna has a realized gain ranging from 2.0 dBi to 9.5 dBi. The efficiency value range from 95.4% to 98.2 %. It is important to note that only simulation data for efficiency are presented due to the limitations of the measurement device. However, the obtained result indicate good performance in terms of efficiency. This is attributed due to the low loss of Rogers RT/Duroid 5880 substrate which a dielectric loss tangent (tan δ) of 0.0009. Furthermore, the envelope correlation coefficient (ECC) of the antenna is illustrated in Fig. 17(b). The EEC value can be calculated using radiation patterns or scattering parameters [4,49,50]. The result shows that the EEC is slightly increased around the S-band. This occurrence is correlated with the MC, as a higher MC between antennas will have a more significant effect on the EEC. Nonetheless, we can see that the ECCs are still under 0.02 at all frequencies. Therefore, it is indicated that the antenna has a small correlation coefficient.

Fig. 18(a-c) show comparison result of diversity gain (DG), total active reflection coefficient (TARC), and channel capacity loss (CCL) of the MIMO antenna C4#, respectively. Moreover, we can also calculate the DG value using the EEC obtained from t adiation patterns. The DG maximum value achieved is 10 dB, while the pr ed MIMO antenna C4# has a high DG of above 9.9 dB. This means the proposed antenna performs well in terms of MIMO performance. Additionally, the TARC value which is a metric to relates the reflection power an N-port microwave compon can be calculated using equations from [4,49,50]. The TARC value of the proposed antenna is lower than −10 dB whi indicates that the reflection power is very low. Then, th L value is lower than 0.4, which is suitable for MIMO applications. Table 2 shows the compa n between our proposed design and previous published antennas. The result shows that the proposed structure has many advantages that are suitable for 5G applications.

Table 2
Performance comparison of the proposed antenna with published antennas.

Ref.	Antenna structure	f_c / BW (GHz)	Proposed application	Size (λ_0)	Substrtae	Shape of rad. pattern	Port	Isolation (dB)	Realized Gain (dBi)	Efficiency (%)	CCL	EEC	DG
[51]	Quasi self complementary	6.85/ 7.50	WLAN, UWB	0.73 × 0.73	FR4, $\varepsilon_r = 4.4$, h = 1.57, tan δ = 0.02	Omni directional	4	< –15	1.7 – 4.2	60–90	N.R	N.R	N.R
[52]	Planar-monopole	7.40/ 9.20	UWB	0.64 × 0.76	RTDuroid4350B, $\varepsilon_r = 3.5$, h = 0.8, tan δ = 0.004	Omni directional	2	< –20	−2 – 5.8	95–99	N.R	N.R	N.R
[53]	Koch fractal monopole	7.5/ 9.0	C-Band, UWB	1.12 × 0.62	FR4, $\varepsilon_r = 4.4$, h = 1.57, tan δ = 0.02	Omni directional	2	< –19	1.0 – 5.0	N.R	N.R	0.17	N.R
[54]	Monopole with floating parasitic	6.85/ 7.50	UWB	0.80 × 0.91	RTDuroid4003, $\varepsilon_r = 4.3$, h = 1.57, tan δ = 0.0024	Omni directional	2	< –16	3.4 – 6.5	N.R	N.R.	0.2	N.R
[55]	Single-dipole	3.65/ 0.30	5G	1.70 × 2.06	FR4, $\varepsilon_r = 4.4$, h = 1, tan δ = 0.02	Directional	2	< –18	N.R.	80–90	N.R.	0.1	N.R.
[56]	Dual monopole	7.55/ 8.90	WLAN and 5G	0.55 × 0.90	RTDuroid5880, $\varepsilon_r = 2.2$, h = 1.57, tan δ = 0.0009	Omni directional	2	< –18	N.R	N.R	N.R	0.35	N.R.
[57]	Monopole with EBG	2.42/ 0.15	WLAN	0.23 × 0.30	FR4, $\varepsilon_r = 4.4$, h = 1, tan δ = 0.02	Directional	2	< –24	− 4.25	50 – 58	N.R	0.008	9.99
[58]	Circular monopole	2.50/ 0.60	WLAN	0.58 × 0.33	JC, $\varepsilon_r = 1.6$, h = 1, tan δ = 0.02	Omni directional	2	< –16	− 3.0	N.R	N.R	0.05	N.R
[59]	CPW Asymmetric EBG	4.75/ 2.90	Sub-6 GHz 5G	0.34 × 0.66	FR4, $\varepsilon_r = 4.4$, h = 1.57, tan δ = 0.02	Omni directional	2	< –18	N.R	N.R	N.R	0.025	− 10.0
[60]	O-shaped monopole	4.10/ 3.40	WLAN and 5G	0.13 × 0.62	FR4, $\varepsilon_r = 4.4$, h = 1.57, tan δ = 0.02	Omni directional	2	< –23	2 – 4	20.0–65.0	N.R	N.R	N.R
[61]	Octagonal-elips shaped	11.0/ 18.0	UWB and 5G	1.46 × 1.61	FR4, $\varepsilon_r = 4.4$, h = 1.57, tan δ = 0.02	Omni directional	2	< –15	− 10.0	90–92	N.R	0.02	9.80–10.00
[62]	Octagonal-shaped radiating	6.85/ 7.50	UWB with nocth	0.43 × 0.68	FR4, $\varepsilon_r = 4.4$, h = 1.57, tan δ = 0.02	Omni directional	2	< –18	1.2 – 2.91	70–90	<0.05	<0.02	9.40–10.00
[63]	Metamaterial and SIW	9.00/ 14.00	UWB	1.05 × 1.08	FR4, $\varepsilon_r = 4.4$, h = 1.57, tan δ = 0.02	Omni directional	2	< –23	3.7 – 4.3	65–80	<0.04	0.04	1.5–10
This paper	Quasi-tapered using circular shaped	14.65/ 22.70	4G / Mid-band 5G / WLAN /X-Band / High band 5G	4.15 × 2.09	RTDuroid5880, $\varepsilon_r = 2.2$, h = 1.57, tan δ = 0.0009	Omni directional	2	< –20	2.0–9.5	95.4 – 98.2	<0.04	<0.02	9.88–10

Note: fc = frequency center, BW = bandwidth, CCL = channel capacity loss, EEC = envelop correlation coefficient, DG = diversity gain, and N.R = not reported.

7. Conclusion

We have successfully designed a quasi-tapered wideband MIMO antenna by combining a circular-shaped patch and an inverted omega ground structure. An expansion of the exponential tapered model was used to investigate the circular-shaped tapered structure. In detail, the proposed antenna is divided into circular divergent and circular convergent-tapered sections. Then, a transmission lines approach was utilized to analyze and optimize the antenna structure. The proposed model was verified by FEM simultion and also step impedance calculation. Moreover, the proposed MIMO antenna can successfully cover the at 4G (3.3 GHz), mid-band 5G (3.4–3.8 GHz), WLAN (5.8 GHz), X-band (10–11 GHz), and high-band 5G (24.5–26 GHz) communications. A good agreement between the simulated and measured results validates the proposed method. A good agreement between the simulated and measured results validates the proposed method.

Declaration of Competing Interest

The authors declare that they have no known competing financial interests or personal relationships that could have appeared to influence the work reported in this paper.

Data availability

Data will be made available on request.

Acknowledgment

This work is supported by the Kementerian Pendidikan, Kebudayaan, Riset, dan Teknologi of Indonesia. Universitas Sultan Ageng Tirtayasa. 2023.

References

[1] B. Aghoutane, S. Das, M. EL Ghzaoui, B. T. P. Madhav, and H. El Faylali, "A novel dual band high gain 4-port millimeter wave MIMO antenna array for 28/37 GHz 5G applications," *AEU - Int. J. Electron. Commun.*, vol. 145, no. December 2021, p. 154071, 2022, https://doi.org/10.1016/j.aeue.2021.154071.

[2] B. Feng, Y. Tu, J. Chen, K. L. Chung, and S. Sun, "High-performance dual circularly-polarized antenna arrays using 3D printing for 5G millimetre-wave communications," *AEU - Int. J. Electron. Commun.*, vol. 130, no. June 2020, p. 153569, 2021, 10.1016/j.aeue.2020.153569.

[3] Yadav V, Yadav RS, Yadav P, Mishra B, Kumar A. "Dual and wideband 6-port MIMO antenna for WiFi, LTE and carrier aggregation systems applications", *AEU -*. Int J Electron Commun 2023;162. https://doi.org/10.1016/j.aeue.2023.154576.

[4] Cuneray K, Akcam N, Okan T, Arican GO. "28/38 GHz dual-band MIMO antenna with wideband and high gain properties for 5G applications", *AEU -*. Int J Electron Commun 2023;vol. 162:154553. https://doi.org/10.1016/j.aeue.2023.154553.

[5] Mao CX, Khalily M, Xiao P, Brown TWC, Gao S. Planar sub-millimeter-wave array antenna with enhanced gain and reduced sidelobes for 5G broadcast applications. IEEE Trans Antennas Propag 2019;67(1):160–8. https://doi.org/10.1109/TAP.2018.2874796.

[6] Di Renna RB, Magri Souza VPR, Ferreira TN, Matos LJ, Souza JAM, Siqueira GL. A new double-sided substrate-integrated waveguide slot array antenna for 5G applications. Microw Opt Technol Lett 2019;61(3):682–7. https://doi.org/10.1002/mop.31617.

[7] Wen S, Dong Y. A low-profile wideband antenna with monopolelike radiation characteristics for 4G/5G indoor micro base station application. IEEE Antennas Wirel Propag Lett 2020;19(12):2305–9. https://doi.org/10.1109/LAWP.2020.3030968.

[8] Sun K, Yang D, Liu S. A wideband hybrid feeding circularly polarized magneto-electric dipole antenna for 5G Wi-Fi. Microw Opt Technol Lett 2018;60(8):1837–42. https://doi.org/10.1002/mop.31259.

[9] Al-Rawi A, Hussain A, Yang J, Franzen M, Orlenius C, Kishk AA. A new compact wideband MIMO antenna - the double-sided tapered self-grounded monopole array. IEEE Trans Antennas Propag 2014;62(6):3365–9. https://doi.org/10.1109/TAP.2014.2309985.

[10] Ma TG, Jeng SK. A printed dipole antenna with tapered slot feed for ultrawideband applications. IEEE Trans Antennas Propag 2005;53(11):3833–6. https://doi.org/10.1109/TAP.2005.858819.

[11] Allen CM, Eldek AA, Elsherbeni AZ, Smith CE, Huang CWP, Lee KF. Dual tapered meander slot antenna for radar applications. IEEE Trans Antennas Propag 2005;53(7):2324–8. https://doi.org/10.1109/TAP.2005.850757.

[12] Ren J, et al. Large Frequency Ratio Vivaldi Antenna System With Low-Frequency Gain Enhancement Utilizing Dual-Function Taper Slot. IEEE Trans Antennas Propag 2022;70(6):4854–9.

[13] Ding T, Wang M, Xiao J, Shu J, Ye Q. A Wrench-Shaped Monopole-Like Slot Antenna For UWB Applications. Cross Strait Radio Science & Wireless Technology Conference (CSRSWTC):9–11. https://doi.org/10.1109/CSRSWTC50769.2020.9372582.

[14] Ling CW, Lo WH, Yan RH, Chung SJ. Planar binomial curved monopole antennas for ultrawideband communication. IEEE Trans Antennas Propag 2007;55(9):2622–4. https://doi.org/10.1109/TAP.2007.904140.

[15] Wang L, et al. Compact UWB MIMO antenna with high isolation using fence-type decoupling structure. IEEE Antennas Wirel Propag Lett 2019;18(8):1641–5. https://doi.org/10.1109/LAWP.2019.2925857.

[16] Nouri M, Abazari Aghdam S, Jafarieh A, Bagby J, Sahebghalam S. A wideband millimeter-wave antenna based on quasi-Yagi antenna with MIMO circular array antenna beamforming for 5G wireless networks. Microw Opt Technol Lett 2019;61(7):1810–4. https://doi.org/10.1002/mop.31790.

[17] Chen HD, Tsai YC, Sim CYD, Kuo C. Broadband eight-antenna array design for Sub-6 GHz 5G NR bands metal-frame smartphone applications. IEEE Antennas Wirel Propag Lett 2020;19(7):1078–82. https://doi.org/10.1109/LAWP.2020.2988898.

[18] Zhao A, Ren Z. Size reduction of self-isolated MIMO antenna system for 5G mobile phone applications. IEEE Antennas Wirel Propag Lett 2019;18(1):152–6. https://doi.org/10.1109/LAWP.2018.2883428.

[19] S. Alam, I. Surjati, A. Ferawan, and T. Firmansyah, "Design and realization of compact microstrip antenna using fractal sierpenski carpet for wireless fidelity application," *Indones. J. Electr. Eng. Informatics*, vol. 6, no. 1, pp. 70–78, 2018, 10.11591/ijeei.v6i1.390.

[20] Multi-output Y.S.M. Three wideband monopolar patch antennas in a Y-shape structure for 5G multi-input–multi-output access points. IEEE Antennas Wirel Propag Lett 2020;19(3):393–7. https://doi.org/10.1109/LAWP.2020.2967354.

[21] Hu WEI, et al. Dual-Band Eight-Element MIMO Array Using Multi-Slot Decoupling Technique for 5G Terminals. IEEE Access 2019;7:153910–20. https://doi.org/10.1109/ACCESS.2019.2948639.

[22] Wibisono G, Firmansyah T. "Concurrent multiband low noise amplifier with multisection impedance transformer", in *Asia-Pacific Microwave Conference Proceedings*. APMC 2012. https://doi.org/10.1109/APMC.2012.6421776.

[23] Hua Q, Huang YI, Member S, Alieldin A. A dual-band dual-polarized base station antenna using a novel feeding structure for 5G communications. IEEE Access 2020;8:63710–7. https://doi.org/10.1109/ACCESS.2020.2984199.

[24] Mohanty A, Sahu S. "Bio-inspired maple-leaf viburnum shaped 4-port compact wideband MIMO antenna with reinforced interleaved SIW cavity integration", *AEU -*. Int J Electron Commun 2022;vol. 156:154383. https://doi.org/10.1016/j.aeue.2022.154383.

[25] Wu T, Wang MJ, Chen J. Decoupling of MIMO antenna array based on half-mode substrate integrated waveguide with neutralization lines. AEU - Int J Electron Commun 2022;157:154416. https://doi.org/10.1016/j.aeue.2022.154416.

[26] Yang SJ, Kim YD, Yun DJ, Yi DW, Myung NH. Antenna modeling using sparse infinitesimal dipoles based on recursive convex optimization. IEEE Antennas Wirel Propag Lett 2018;17(4):662–5. https://doi.org/10.1109/LAWP.2018.2810289.

[27] S. Lin, H. Dong, Y. Liu, X. Y. Zhang, and X. Zhang, "Equivalent Circuit Modeling and Radiation Analysis of a Micro-Coaxial Collinear Antenna," *2022 IEEE Int. Symp. Antennas Propag. Usn. Radio Sci. Meet. AP-S/URSI 2022 - Proc.*, pp. 199–200, 2022, 10.1109/AP-S/USNC-URSI47032.2022.9886416.

[28] Gómez-Tagle J, Christodoulou CG. Extended cavity model analysis of stacked microstrip ring antennas. IEEE Trans Antennas Propag 1997;45(11):1626–35. https://doi.org/10.1109/8.650074.

[29] Wang CJ, Chen LT. Modeling of stepped-impedance slot antenna. IEEE Trans Antennas Propag 2014;62(2):955–9. https://doi.org/10.1109/TAP.2013.2291906.

[30] S. Koziel, S. Ogurtsov, and J. P. Jacobs, "Modeling of wideband antennas using space-mapping-corrected kriging surrogates," *2013 7th Eur. Conf. Antennas Propagation, EuCAP 2013*, pp. 1540–1543, 2013.

[31] Lu G, Korisch I, Greenstein L, Spasojevic P. "Antenna modelling using linear elements, with applications to UWB", *IEEE Antennas Propag.* Soc AP-S Int Symp 2004;3:2544–7. https://doi.org/10.1109/aps.2004.1331892.

[32] Nayak U, Chongder P, Biswas A. "Novel filtering and diplexing linear tapered slot antenna with high-selectivity", *AEU -*. Int J Electron Commun 2022;156. https://doi.org/10.1016/j.aeue.2022.154363.

[33] Roblin C, D'Errico R. Statistical analysis of a parametric model of a 'population' of UWB antennas. Eur Conf Antennas Propagation, EuCAP 2009:3343–7.

[34] Wallace JW, Mehmood R. On the accuracy of equivalent circuit models for multi-antenna systems. IEEE Trans Antennas Propag PART 1 2012;vol. 60(2):540–7. https://doi.org/10.1109/TAP.2011.2152339.

[35] Papamichael V, Soras C. MIMO antenna modelling using the effective length matrices. Prog Electromagn Res C 2009;10:111–27. https://doi.org/10.2528/PIERC09061903.

[36] Papamichael VC. Eigen-analysis of lossy compact multielement antenna systems. IEEE Antennas Wirel Propag Lett 2009;8:1334–6. https://doi.org/10.1109/LAWP.2009.2038288.

[37] S. Kareemulla and V. Kumar, "Diversity performance of band notched ultra-wideband MIMO antenna," *Optik*, vol. 272, no. August 2022, p. 170128, 2023, https://doi.org/10.1016/j.ijleo.2022.170128.

[38] F. Wang, Z. Duan, Q. Li, Y. Wei, and Y. Gong, "Compact wideband MIMO antenna for 5G communication," *2017 IEEE Antennas Propag. Soc. Int. Symp. Proc.*, vol. 2017-Janua, no. c, pp. 939–940, 2017, 10.1109/APUSNCURSINRSM.2017.8072512.

[39] Chen Z, Yuan XT, Ren J, Yuan T. "An ultra-wideband MIMO antenna for 5G smartphone", *AEU -*. Int J Electron Commun 2022;vol. 154:154301. https://doi.org/10.1016/j.aeue.2022.154301.
[40] Ansarizadeh M, Ghorbani A, Abd-Alhameed RA. An approach to equivalent circuit modeling of rectangular microstrip antennas. Prog Electromagn Res B 2008;8:77–86. https://doi.org/10.2528/pierb08050403.
[41] Adams JJ, Bernhard JT. Broadband equivalent circuit models for antenna impedances and fields using characteristic modes. IEEE Trans Antennas Propag 2013;61(8):3985–94. https://doi.org/10.1109/TAP.2013.2261852.
[42] N. M. Din, C. K. Chakrabarty, A. Bin Ismail, K. K. A. Devi2, and W.-Y. Chen, "Design of RF Energy Harvesting System for energizing low power devices," *Prog. Electromagn. Res.*, vol. 132, no. July, pp. 49–69, 2012.
[43] Devi KKA, Sadasivam S, Din NM, Chakrabarthy CK, Rajib SK. Design of a wideband 377 Ohm E-Shaped patch antenna for RF energy harvesting. Microw Opt Technol Lett 2013;55(3):569–73. https://doi.org/10.1002/mop.
[44] Iqbal A, Saraereh OA, Ahmad AW, Bashir S. Mutual Coupling Reduction Using F-Shaped Stubs in UWB-MIMO Antenna. IEEE Access 2017;6:2755–9. https://doi.org/10.1109/ACCESS.2017.2785232.
[45] Technologies L. SMA Connectors [Online]. Available: SMA Connectors 2012. https://www.hasco-inc.com/categories/connectors/sma-connectors.html.
[46] Chang TN, Lin JM. Dual-band circularly polarized monopole antenna. J Electromagn Waves Appl 2015;29(7):843–57. https://doi.org/10.1080/09205071.2015.1022265.
[47] Liang Z, Li Y, Long Y. Multiband monopole mobile phone antenna with circular polarization for GNSS application. IEEE Trans Antennas Propag 2014;62(4):1910–7. https://doi.org/10.1109/TAP.2014.2299821.
[48] M. H. Shih, K. L. Hsiao, and C. J. Wang, "A monopole antenna with circular polarization," *ISAP 2014 - 2014 Int. Symp. Antennas Propagation, Conf. Proc.*, pp. 609–610, 2015, 10.1109/ISANP.2014.7026798.
[49] Li Y, et al. "Mutual coupling reduction for monopole MIMO antenna using L-shaped stubs, defective ground and chip resistors", *AEU -*. Int J Electron Commun 2023;vol. 160:154524. https://doi.org/10.1016/j.aeue.2022.154524.
[50] A. Khan, A. Wakeel, L. Qu, and Z. Zahid, "Dual-band 8 × 8 MIMO antenna with enhanced isolation and efficiency for 5G smartphone applications," *AEU - Int. J. Electron. Commun.*, vol. 163, no. December 2022, p. 154600, 2023, 10.1016/j.aeue.2023.154600.
[51] Liu L, Cheung SW, Yuk TI. Compact MIMO antenna for portable devices in UWB applications. IEEE Trans Antennas Propag 2013;61(8):4257–64. https://doi.org/10.1109/TAP.2013.2263277.
[52] Zhu J, Li S, Feng B. Compact dual-polarized UWB quasi-self-complementary MIMO / Diversity. IEEE Antennas Wirel Propag Lett 2016;15:905–8. https://doi.org/10.1109/LAWP.2015.2479622.
[53] Irene G, Rajesh A. A penta-band reject inside cut Koch fractal hexagonal monopole UWB MIMO antenna for portable devices. Prog Electromagn Res C 2018;82:225–35. https://doi.org/10.2528/pierc18020604.
[54] Khan MS, Capobianco A, Najam AI, Shoaib I, Autizi E, Shafique MF. Compact ultra-wideband diversity antenna with a floating parasitic digitated decoupling structure. IET Microwaves, Antennas Propag 2014;8(10):747–53. https://doi.org/10.1049/iet-map.2013.0672.
[55] Qu L, Piao H. A dual-port single-dipole MIMO antenna pair based on selective modal excitation for 5G metal-rimmed terminals. IEEE Access 2022;10:100208–14. https://doi.org/10.1109/ACCESS.2022.3188017.
[56] A. Quddus and R. Saleem, "Dual Port UWB Diversity/MIMO Antenna with Dual Band-Notch Characteristics," in *International Conference on Signal Processing and Communication Systems (ICSPCS)*, 2016, pp. 7–10. https://doi.org/10.1109/ICSPCS.2016.7843320.
[57] Sharma K, Pandey GP. Two port compact MIMO antenna for ISM band applications. Prog Electromagn Res C 2020;100:173–85. https://doi.org/10.2528/pierc20011504.
[58] Raviteja GV, Kumar PP, Ramesh G, Prasad BG, Sai RV. Wearable Dual-port MIMO antenna for On-body applications," in *International Conference on Elect*. Electron Inform Commun Technol (ICEEICT) 2022:7–11. https://doi.org/10.1109/ICEEICT53079.2022.9768416.
[59] A. I. Afifi, A. S. Abd El-Hameed, A. Allam, S. M. Ahmed, and A. B. Abdel-Rahman, "Dual Port MIMO Antenna with Low Mutual Coupling Based on Asymmetric EBG Decoupling Structure," *15th Eur. Conf. Antennas Propagation, EuCAP 2021*, pp. 5–9, 2021, 10.23919/EuCAP51087.2021.9411149.
[60] Soltani S, Lotfi P, Murch RD. Design of compact dual-band dual-port WLAN MIMO antennas using slots. IEEE Antennas Propag Soc AP-S Int Symp 2015;vol. 2015:924–5. https://doi.org/10.1109/APS.2015.7304849.
[61] Gireesh P, Sandeep Kumar P, Malathi K, Khanra I, Agarwal A, Sivakumar K. Design and analysis of dual port super wideband antenna set for MIMO applications. J Phys Conf Ser 2021;1964(6):pp. https://doi.org/10.1088/1742-6596/1964/6/062051.
[62] Kumar A, Ansari AQ, Kanaujia BK, Kishor J, Kumar S. An ultra-compact two-port UWB-MIMO antenna with dual band-notched characteristics. AEU - Int J Electron Commun 2020;114:152997. https://doi.org/10.1016/j.aeue.2019.152997.
[63] Anand S, Theetharappan R. "Metamaterial and SIW inspired isolating fences for lateral de-coupling in MIMO antenna", *AEU -*. Int J Electron Commun 2023;vol. 166:154667. https://doi.org/10.1016/j.aeue.2023.154667.

Modeling of quasi-tapered microstrip antenna based on expansion-exponential tapered method and its application for wideband MIMO structure

ORIGINALITY REPORT

18%	13%	16%	%
SIMILARITY INDEX	INTERNET SOURCES	PUBLICATIONS	STUDENT PAPERS

PRIMARY SOURCES

1	Michael Kerr, Fengling Han, Xun Yi, Andrei Kelarev, Ron Van Schyndel. "A non-invasive method for the cataloguing and authentication of surveillance video using on-camera blockchain participation, machine learning and signal analysis", Forensic Science International: Digital Investigation, 2023 Publication	1%
2	ebin.pub Internet Source	1%
3	faculty.ksu.edu.sa Internet Source	1%
4	"Optical and Wireless Technologies", Springer Science and Business Media LLC, 2020 Publication	1%
5	academic.hep.com.cn Internet Source	1%
6	livrepository.liverpool.ac.uk Internet Source	1%

7	www.hindawi.com Internet Source	1 %
8	dspace.dtu.ac.in:8080 Internet Source	<1 %
9	eprints.untirta.ac.id Internet Source	<1 %
10	Jin Cheng, Robert J. Adams, John C. Young, Michael A. Khayat. "Augmented EFIE With Normally Constrained Magnetic Field and Static Charge Extraction", IEEE Transactions on Antennas and Propagation, 2015 Publication	<1 %
11	A. Moradikordalivand, T. A. Rahman, S. Ebrahimi, S. Hakimi. "An Equivalent Circuit Model for Broadband Modified Rectangular Microstrip-Fed Monopole Antenna", Wireless Personal Communications, 2014 Publication	<1 %
12	www.freepatentsonline.com Internet Source	<1 %
13	Ultra-Wideband Short Pulse Electromagnetics 9, 2010. Publication	<1 %
14	curve.carleton.ca Internet Source	<1 %
	hal.archives-ouvertes.fr	

15	Internet Source	<1%
16	www.scilit.net Internet Source	<1%
17	Majid Shokri, Changiz Ghobadi, Javad Nourinia, Pedro Pinho et al. "A Compact Four Elements Self-Isolated MIMO Antenna for C-Band Applications", 2023 IEEE 27th Workshop on Signal and Power Integrity (SPI), 2023 Publication	<1%
18	Wu, J., Z. Zhao, Z. Nie, and Q. Liu. "A Broadband Unidirectional Antenna Based on Closely Spaced Loading Method", IEEE Transactions on Antennas and Propagation, 2012. Publication	<1%
19	eprints.utem.edu.my Internet Source	<1%
20	thesai.org Internet Source	<1%
21	ijece.iaescore.com Internet Source	<1%
22	Yue Zhao. "A N77/78/79 Self-Decoupled Antenna Pair for 5G Smartphones", 2020 IEEE Asia-Pacific Microwave Conference (APMC), 2020 Publication	<1%

23	aces-society.org Internet Source	<1%
24	aemjournal.org Internet Source	<1%
25	doaj.org Internet Source	<1%
26	Lisong Zhang, Yun Xie, Xiangzhen Yan, Xiujuan Yang. "An elastoplastic semi-analytical method to analyze the plastic mechanical behavior of buried pipelines under landslides considering operating loads", Journal of Natural Gas Science and Engineering, 2016 Publication	<1%
27	Abdelhamid M. H. Nasr, Amr M. E. Safwat. "Multimode Coplanar Waveguide Cross-Junction: Equivalent Circuit Model and Air-Bridge Free Applications", IEEE Transactions on Microwave Theory and Techniques, 2017 Publication	<1%
28	Manish Sharma, Sukhbir Singh, Ranjit Varma. "Computational Design, Analysis and Characterization of Beetle Shaped High Isolation Multiple-Input-Multiple-Output Reconfigurable Monopole-Antenna with Dual Band Filters for Wireless Applications", Wireless Personal Communications, 2021 Publication	<1%

29	Yuehui Gao, Junlin Wang, Xin Wang, Rui Shao. "Miniaturized MIMO Antenna Array with High Isolation for 5G Metal-Frame Smartphone Application", Micromachines, 2022 Publication	<1 %
30	www.sciencepublishinggroup.com Internet Source	<1 %
31	Mahdi Nouri, Sajjad Abazari Aghdam, Alireza Jafarieh, Jonathan Bagby, Sara Sahebghalam. "A wideband millimeter - wave antenna based on quasi - Yagi antenna with MIMO circular array antenna beamforming for 5G wireless networks", Microwave and Optical Technology Letters, 2019 Publication	<1 %
32	Shuang Luo, Daiqiang Wang, Yuqing Chen, Ershi Li, Chong Jiang. "A compact dual-port UWB-MIMO antenna with quadruple band-notched characteristics", AEU - International Journal of Electronics and Communications, 2021 Publication	<1 %
33	Syah Alam, Zahriladha Zakaria, Indra Surjati, Noor Azwan Shairi, Mudrik Alaydrus, Teguh Firmansyah. "Multifunctional of Dual-Band Permittivity Sensors with Antenna using Multicascode T-shaped Resonators for Simultaneous Measurement of Solid Materials	<1 %

	and Data Transfer Capabilities", Measurement, 2023 Publication	
34	journals.pen2print.org Internet Source	<1 %
35	jpier.org Internet Source	<1 %
36	opus.lib.uts.edu.au Internet Source	<1 %
37	web.ece.ucsb.edu Internet Source	<1 %
38	Heba Aboelleil, Ahmed A. Ibrahim, Ashraf A. M. Khalaf. "A compact multiple-input multiple-output antenna with high isolation for wireless applications", Analog Integrated Circuits and Signal Processing, 2021 Publication	<1 %
39	S. Rajkumar, Krishnasamy T. Selvan, P.H. Rao. "Compact 4 element Sierpinski Knopp fractal UWB MIMO antenna with dual band notch", Microwave and Optical Technology Letters, 2018 Publication	<1 %
40	harvest.usask.ca Internet Source	<1 %
41	www.research-collection.ethz.ch Internet Source	

<1%

42 Amit Kumar, Abdul Quaiyum Ansari, Binod Kumar Kanaujia, Jugul Kishor, Sachin Kumar. "An ultra-compact two-port UWB-MIMO antenna with dual band-notched characteristics", AEU - International Journal of Electronics and Communications, 2020
Publication

<1%

43 Kuiwen Xu, Fei Liu, Liang Peng, Wen-Sheng Zhao, Lixin Ran, Gaofeng Wang. "Multi-mode and Wideband Printed Loop Antenna Based on Degraded Split-Ring Resonators", IEEE Access, 2017
Publication

<1%

44 Praveen Kumar, Rashmi Sinha, Arvind Choubey, Santosh Kumar Mahto. "DGS based miniaturized wideband MIMO antenna with efficient isolation for C band applications", Frequenz, 2023
Publication

<1%

45 Samir Salem Al-Bawri, Mohammad Tariqul Islam, Tayyab Shabbir, Ghulam Muhammad, Md Shabiul Islam, Hin Yong Wong. "Hexagonal Shaped Near Zero Index (NZI) Metamaterial Based MIMO Antenna for Millimeter-Wave Application", IEEE Access, 2020
Publication

<1%

46	Xiao-Ting Yuan, Wei He, Kai-Dong Hong, Chong-Zhi Han, Zhe Chen, Tao Yuan. "Ultra-Wideband MIMO Antenna System with High Element-Isolation for 5G Smartphone Application", IEEE Access, 2020 Publication	<1 %
47	repository.kaust.edu.sa Internet Source	<1 %
48	Ashim Kumar Biswas, Ujjal Chakraborty. "Compact wearable MIMO antenna with improved port isolation for ultra-wideband applications", IET Microwaves, Antennas & Propagation, 2019 Publication	<1 %
49	Huy Hung Tran, Niamat Hussain, Tuan Tu Le. "Low-profile wideband circularly polarized MIMO antenna with polarization diversity for WLAN applications", AEU - International Journal of Electronics and Communications, 2019 Publication	<1 %
50	M. Nirmala, D. Venusree, B. Aakash, B. Meghana, V. S. Manidhar. "A Decoupled Dual Element Reconfigurable MIMO Antenna with Improved Isolation for Wireless Applications", 2021 12th International Conference on Computing Communication and Networking Technologies (ICCCNT), 2021	<1 %

Publication

51	Nour Elhouda Nasri, Sudipta Das, Mohammed El Ghzaoui, Boddapati Taraka Phani Madhav, Samudrala Vara Kumari, Mohammed Fattah. "A Compact Wideband (22–44GHz) Printed 2 × 4 MIMO Array Antenna with High Gain for 26/28/38GHz Millimeter-Wave 5G Applications", Journal of Circuits, Systems and Computers, 2023 Publication	<1 %
52	Sachin Kumar, Gwan H. Lee, Dong H. Kim, Wahab Mohyuddin, Hyun C. Choi, Kang W. Kim. "Multiple ‐ input ‐ multiple ‐ output/diversity antenna with dual band ‐ notched characteristics for ultra ‐ wideband applications", Microwave and Optical Technology Letters, 2019 Publication	<1 %
53	Vishal Sorathiya, Abdullah G. Alharbi, Sunil Lavadiya. "Design and investigation of unique shaped low-Profile material-based superlative two-element printed ultrawideband MIMO antenna for Zigbee/WiFi/5G/WiMAX applications", Alexandria Engineering Journal, 2022 Publication	<1 %
54	Wen Jiang, Yangqiang Cui, Bo Liu, Wei Hu, Yan Xi. "A Dual-Band MIMO Antenna With	<1 %

Enhanced Isolation for 5G Smartphone Applications", IEEE Access, 2019
Publication

55	Yikai Chen, Chao-Fu Wang. "Characteristic Modes", Wiley, 2015 Publication	<1 %
56	acikerisim.medipol.edu.tr Internet Source	<1 %
57	link.springer.com Internet Source	<1 %
58	onlinelibrary.wiley.com Internet Source	<1 %
59	www.eucap2021.org Internet Source	<1 %
60	www2.mdpi.com Internet Source	<1 %
61	Cheung, Sing Wai, Li Liu, and Tung Ip Yuk. "Compact multiple-input–multiple-output antenna using quasi-self-complementary antenna structures for ultrawideband applications", IET Microwaves Antennas & Propagation, 2014. Publication	<1 %
62	Hossein Malekpoor, Ali Abolmasoumi. "High - isolated broadband eight - element linear multi - input multi - output array over	<1 %

artificial magnetic surface for wireless and sub ‐ 6GHz 5G communications", International Journal of Communication Systems, 2022
Publication

---

63 Kutay Cuneray, Nursel Akcam, Tayfun Okan, Galip Orkun Arican. "28/38 GHz dual-band MIMO antenna with wideband and high gain properties for 5G applications", AEU - International Journal of Electronics and Communications, 2023
Publication

<1%

---

64 PARTHASARATHY RAMANUAJAM, Chandrasekar Arumugam, Manimaran Ponusamy, Ramesh P G V. "Design of Compact patch Antenna with Enhanced Gain and Bandwidth for 5G mm-Wave Applications", IET Microwaves, Antennas & Propagation, 2020
Publication

<1%

---

65 Saeid Karamzadeh, Bal. S. Virdee, Vahid Rafii, Mesut Kartal. "Circularly polarized slot antenna array with sequentially rotated feed network for broadband application", International Journal of RF and Microwave Computer-Aided Engineering, 2015
Publication

<1%

66	Xiao Zhang, Qi-Yu Zeng, Zeng-Pei Zhong, Qiong-Sen Wu, Lei Zhu, Tao Yuan, Qing-Hua Jiang, Bo Mei. "Analysis and Design of Stable-Performance Circularly-Polarized Antennas Based on Coupled Radiators for Smart Watches", IEEE Transactions on Antennas and Propagation, 2022 Publication	<1 %
67	Yanxiu Li, Li-an Bian, Kai-da Xu, Yu Liu, Yaokun Wang, Ranhao Chen, Shu Xie. "Mutual coupling reduction for monopole MIMO antenna using L-shaped stubs, defective ground and chip resistors", AEU - International Journal of Electronics and Communications, 2023 Publication	<1 %
68	Zhang, Shuai, and Gert Pedersen. "Mutual Coupling Reduction for UWB MIMO Antennas with a Wideband Neutralization Line", IEEE Antennas and Wireless Propagation Letters, 2015. Publication	<1 %
69	dokumen.pub Internet Source	<1 %
70	dro.dur.ac.uk Internet Source	<1 %
71	ejournal.radenintan.ac.id Internet Source	

		<1%
72	res.mdpi.com Internet Source	<1%
73	www.sciencepubco.com Internet Source	<1%
74	www.slideshare.net Internet Source	<1%
75	Kamel Salah Sultan, Haythem Hussein Abdullah. "PLANAR UWB MIMO-DIVERSITY ANTENNA WITH DUAL NOTCH CHARACTERISTICS", Progress In Electromagnetics Research C, 2019 Publication	<1%
76	mdpi.com Internet Source	<1%
77	"Advances in VLSI, Communication, and Signal Processing", Springer Science and Business Media LLC, 2021 Publication	<1%
78	Abdessalam El Yassini, Saida Ibnyaich, Truong Khang Nguyen, Abdelouhab Zeroual. "Design and analysis of single and multi‐input multioutput triple‐band metamaterial inspired antennas for WiMAX, WLAN, and	<1%

satellite applications", International Journal of Communication Systems, 2022
Publication

79 Amjad Iqbal, Abdul Basir, Amor Smida, Nazih Khaddaj Mallat, Issa Elfergani, Jonathan Rodriguez, Sunghwan Kim. "Electromagnetic Bandgap Backed Millimeter-Wave MIMO Antenna for Wearable Applications", IEEE Access, 2019 <1%
Publication

80 Saswati Ghosh, Ajay Chakrabarty. "Dual Band Circularly Polarized Monopole Antenna Design for RF Energy Harvesting", IETE Journal of Research, 2015 <1%
Publication

Exclude quotes	Off	Exclude matches	Off
Exclude bibliography	On		

Modeling of quasi-tapered microstrip antenna based on expansion-exponential tapered method and its application for wideband MIMO structure

GRADEMARK REPORT

FINAL GRADE

/0

GENERAL COMMENTS

Instructor

PAGE 1

PAGE 2

PAGE 3

PAGE 4

PAGE 5

PAGE 6

PAGE 7

PAGE 8

PAGE 9

PAGE 10

PAGE 11

PAGE 12

PAGE 13

PAGE 14